A Simplified FE Model of the Four-Ball Tester for Evaluating Stress and Strain Distributions

Catalin PIRVU*,[1], Traian Florian IONESCU[2], Lorena DELEANU*,[2,3], Constantin GEORGESCU[2]

*Corresponding authors
[1]INCAS – National Institute for Aerospace Research "Elie Carafoli",
220 Iuliu Maniu, Bucharest 061126, Romania,
pirvu.catalin@incas.ro*
[2]"Dunarea de Jos University" of Galati,
111 Domnească, Galati 800008, Romania
[3]Technical Sciences Academy of Romania (ASTR),
030167, Bucharest, Romania,
lorena.deleanu@ugal.ro*

DOI: 10.13111/2066-8201.2026.18.1.6

Received: 18 December 2025/ Accepted: 22 February 2026/ Published: March 2026
Copyright © 2026. Published by INCAS. This is an "open access" article under the CC BY-NC-ND license (http://creativecommons.org/licenses/by-nc-nd/4.0/)

Abstract: *This paper presents a simplified isothermal FE model of the four-ball tribotester in order to analyze stress and strain distributions, in mixt or boundary lubrication regime, for a range of loads and friction coefficients and the transition from a normal mild regime (acceptable load, very small permissible local plastic strain) to a severe regime (identifying maximum von Mises stress and plastic strain). The model consists of only two balls, in their actual position, the load being applied to the rotating ball and supported by the second, stationary ball. The equivalence of model loading is done by the displacement (approach) between the rotating ball and the stationary ball, identical to that obtained from tests. The constitutive model of ball material is based on experimental results reported in literature for the same steel grade. Research limitations are related to the mixt regime simulation (here characterized by a friction coefficient and not including a fluid film, the values experimentally obtained for the friction coefficient in mixt regime being in the selected range of the simulation). The effect of roughness is neglected by considering smooth bodies. The simulation was run for three values of friction coefficient (0.0, 0.08 and 0.1, respectively), pointing out its influence on stress and strain distributions. The model highlights the ellipsoidal shape of the indentation on the stationary ball, due to friction and particular sliding. It was found that strain and stress are induced from the first rotation of the tribosystem, if the system is statically loaded before starting sliding (as it happens in the actual test) and differences between strain and stress distributions are obvious for cases with friction (friction coefficient was considered constant) and the case without friction.*

Key Words: *FE model, four-ball tribotester, friction, stress distribution, plastic strain distribution, friction coefficient*

1. INTRODUCTION

The issue of elasto-plastic contact can be formulated by an elastic problem, over which a plastic (residual) problem is superposed [1–10]. When the applied load causes stresses that exceed the yield limit of the ball material, in certain zones of the bodies in contact, it results:

- the generation of a field with plastic strains, obviously remaining after unloading,
- the plastic imprint increases the contact conformability, thus reducing the local stress,
- the change of the contact geometry leads to the change of the stress distribution on the contact surface and, implicitly, in the volume around it.

Existing studies [11–22] showed that, as compared to the elastic contact, the contact solution for the elasto-plastic contact has two main characteristics: the maximum contact stress was lower and different in distribution and the contact radius was larger as compared to simply elastic models.

Hardy et al. [22] assumed that, when a plastic strain occurred in the contact area, the maximum contact stress tended to be constant. This implies the existence of a limit value of the maximum contact stress in the elasto-plastic contact, which should be proportional to the yield limit of materials in contact.

The aim of this study is to simulate the behavior of the four-ball tester on a simplified finite element model (two balls in contact, but identically loaded as in the actual system), in order to point out changes in stress and strain distributions, the calculated values being useful for establishing the boundary between a normal regime and a severe one. Even if lubrication is not included in the model, the introduction of a friction coefficient with values obtained in actual tests on the four-ball machines [24–26] could reflect well the contact loading in mixt or boundary regime that the lubricant generates under high loads.

2. MATERIALS AND METHODS

Unlike Hooke's relation that supposes a direct proportionality between stress and strain, in the elasto-plastic field, the stress-strain relation is nonlinear, usually mathematically modeled based on experimental data and of simpler or more complex form, depending on factors such as temperature, strain rate, etc. [9, 27].

Given the multitude of materials, structures and demands, a valid general model is difficult to achieve and impractical. Therefore, in this study, the authors evaluate the behavior of the material the balls are made of, with a bilinear hardening model, based on experimental data reported in [28], for the steel grade 100Cr6, hardened up to 65 HRC. For hard steels, as is the case of ball bearing steel, the yield limit can be considered identical to the elastic limit.

For an elasto-plastic contact, the hypothesis that implies the cumulation of the elastic effect with the plastic one is accepted as:

$$\varepsilon = \varepsilon_e + \varepsilon_p \tag{1}$$

where ε_e represents the elastic strain and ε_p is the plastic strain, in the same location, the modulus of elasticity being considered as constant.

The model simplification consists of the fact that it is made of only two balls, but their position is the actual location on the tribotester, the load being applied in the vertical direction, on the rotating ball, and it is offset by the second ball (stationary). The equivalence of model loading is done by the displacement (approach) between the upper rotating ball and the lower stationary ball, a displacement identical to that obtained from the laboratory tests. This vertical displacement is calculated as follows:

- the position of the initial contact between the upper and lower ball is geometrically determined, without loading,
- the displacement between the two balls in the direction of the centers is calculated, depending on vertical load,

- the projection of the displacement on the vertical axis is also calculated; the displacement on the center line of the two spheres is composed of the height of the cap corresponding to the average wear scar diameter (WSD) (as determined in [26]), to which the depth of the wear scar is added, as determined by 2D profiles, measured perpendicular to the sliding direction.

The model is run in Ansys (Explicit Dynamics) and the simulation has two stages:

1. the stage of loading of the two balls, in static conditions,
2. the stage of performing a rotation or a part of rotation, under the load, so that the resulting imprint during sliding with friction does not overlap with the initial imprint between spheres.

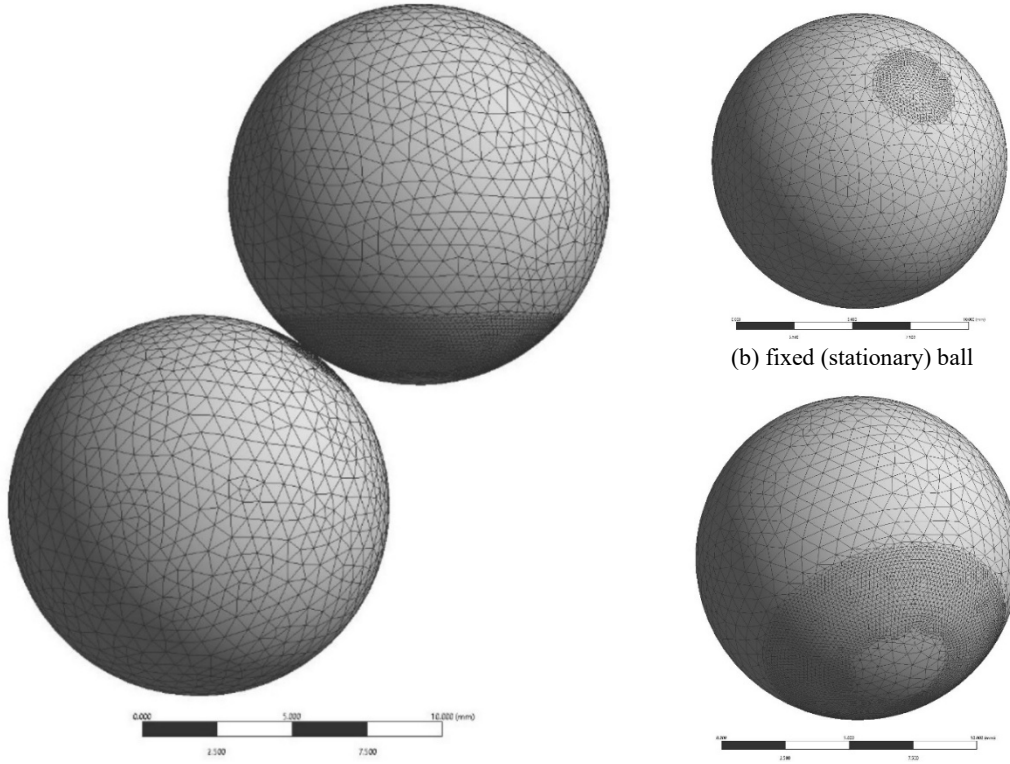

(a) model mesh (overview) (b) fixed (stationary) ball (c) rotating ball

Fig. 1 Details of contact area mesh: (a) model mesh (overview); (b) fixed (stationary) ball; (c) rotating ball

For this finite element model, the simplifying hypotheses are:

- isothermal regime, because temperature measurements in the oil bath at the end of the tests showed that the temperature did not exceed 90 ºC, as reported by David [23], Cristea [24], Georgescu [25] and Șolea [29], which means that the properties of the hardened steel balls are not affected (ball bearing steel has a tempering temperature of about 300 ºC; thus, the structure and properties of the steel can be considered as not being thermally influenced),
- the friction coefficient is specific to boundary or mixt lubrication (COF = 0.08...0.15), as recorded by testing in [26, 29],
- modeling without lubrication, but introducing measured values of the friction coefficient as obtained in the lubricant presence in actual tests, denotes the existence of a mixed regime and, therefore, a lower influence of a partial fluid film,
- perfectly smooth bodies in contact; this can be accepted as very small values of the initial roughness parameters emerge from the profilometric study of the balls [24, 26],

- wear is not taken into account; this may affect the simulation results, but for assessing of stress and strain, in the severe regime, wear is taken into consideration by the approach between balls, larger when ball material is lost. The 2D profilometric study in the severe regime shows that abrasive wear is more observable at low loads and plastic strain, without a severe abrasive wear, is observable at high loads (850 N, 900 N),
- an elasto-plastic constitutive model for the ball steel; the authors selected a bilinear-isotropic model with hardening, based on experimental data provided by Guo and Liu [28].

The two spheres in contact are represented in Fig. 1(a). The initial position of these balls is identical to that of actual balls of the four-ball tribotester.

Figures 2(b) and (c) present details of the mesh. A finer mesh network of the contact areas was done on the stationary ball and on a spherical sector corresponding to a band larger than the friction path on the rotating ball.

Adaptive convergence denotes the condition in which the computed structural response, specifically the equivalent von Mises stress, approaches a mesh-independent value as the discretization is refined. The assessment is performed by sequentially running the model with progressively finer meshes (Fig. 2) and quantifying the variation of the response within a designated region of interest, here the contact zone.

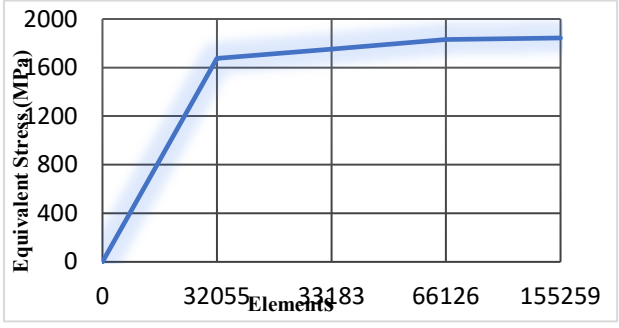

Fig. 2 The convergence process taking into account the maximum value of equivalent stress for the simulation process

Convergence is deemed to be achieved when the relative change in the monitored stress metric between consecutive refinement levels (see Fig. 3) falls below the prescribed tolerance (here, a maximum allowable deviation of 5%).

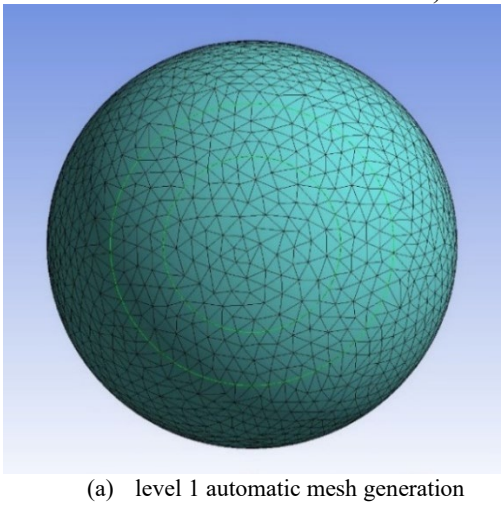

(a) level 1 automatic mesh generation

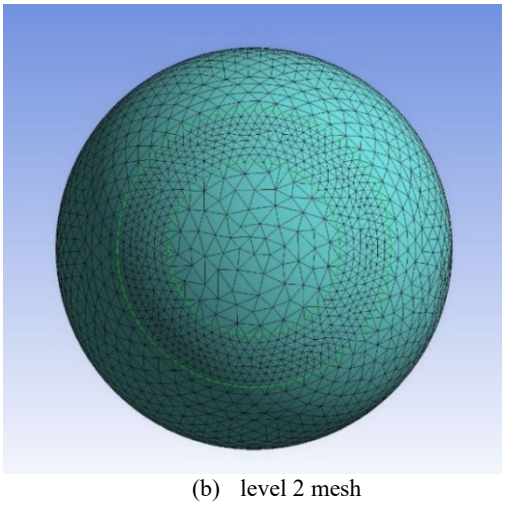

(b) level 2 mesh

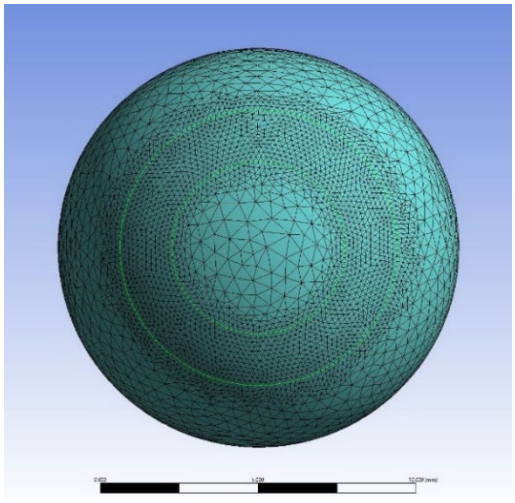

(c) level 3 mesh

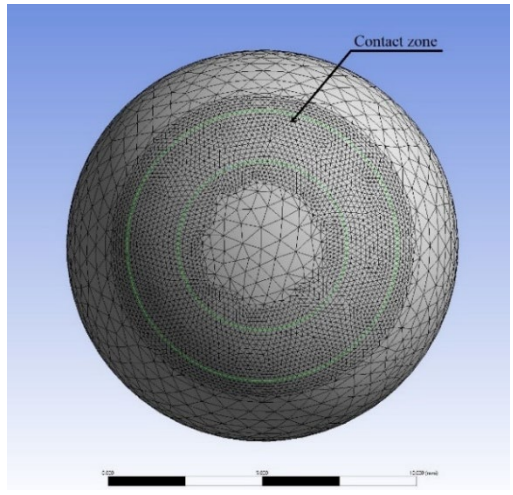

(d) level 4 refined mesh

Fig. 3 Mesh configurations for the rotating ball in the contact zone

Under these conditions, the solution can be considered numerically stable and sufficiently accurate from level 3 onward for the defined analysis objectives, as shown in Table 1. However, taking into account the users' experience and the need for a finer mesh in the contact region to improve visualization of the interaction between the two balls, a smoother (more refined) mesh is recommended (Fig. 3(d)).

Table 1. Mesh characteristics for the model

	Maximum equivalent stress in contact zone (MPa)	Variation with reference to consecutive case (%)	Elements of the entire model
1	1675	-	32,055
2	1752.9	4.54	33,183
3	1831.8	4.30	66,126
4	1843.7	0.64	155,259

For the final model, the mesh consists of 155,259 elements. The element transition ratio is 0.272, and the element growth rate is 1.2.

Table 2 gives the characteristics for the ball material. Table 3 gives the values of the characteristic points on the strain-stress bilinear hardening model for the ball steel.

Table 2. Material properties (for the model proposed by the author) [27]

Properties	**Value**
Density	7,850 (kg·m^{-3})
Young's modulus	2×10^5 (MPa)
Poisson's ratio	0.3
Volume modulus	1.6667×10^5 (MPa)
Shear modulus	0.76923×10^5 (MPa)

Table 3. Characteristic points on the strain-stress curve for ball steel constitutive model

Points	**Stress (MPa)**	**Strain (mm/mm)**
Yield point	1400	$7\cdot10^{-3}$
Strength limit	1850	$1.1\cdot10^{-2}$

The simulation stages are pointed out on a von Mises stress (maximum values) – time curve, in Fig. 4:

- stage 1: a constant slope load is applied on the two balls until the displacement in the z direction of the model is sufficiently close to the actual displacement of the four-ball system,
- stage 2: the upper ball, keeping the vertical axis fixed, performs a complete (360º for lower loads), or incomplete (300º) rotation, for higher loads (in order to have no overlapping of the friction path); it performs a complete rotation in 1.006 seconds (corresponding to the test sliding velocity of 0.53 m/s or 1400 rpm).

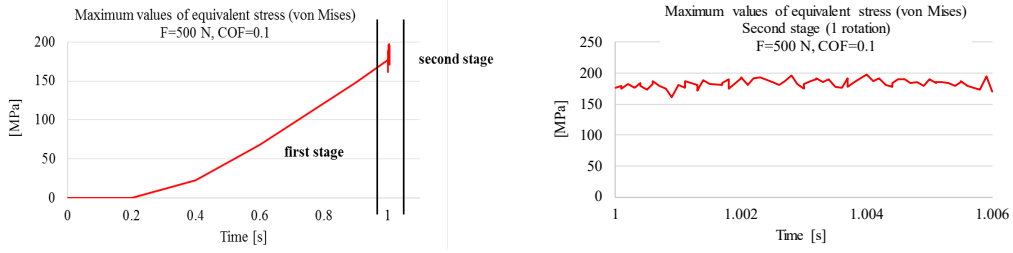

Fig. 4 Identification of the simulation stages, here being represented by the evolution in time of the maximum von Mises stress, for F = 500 N, COF = 0.1 (load is equivalent to a vertical approach z = 0.0065 mm): (a) maximum equivalent stress during the entire simulation, made of two stages; (b) detail of the second stage

The geometry of the model is presented in Fig. 5, with only two balls (the upper ball that rotates and the bottom ball that is fixed), the balls being in contact without deformation and wear. Fig. 6 presents the components of the vertical displacements, $\delta_1+\delta_2$ being the approach between the two balls on normal direction in contact (H is the height of the equilateral triangle $O_1O_2O_3$, obtained for the centers of fixed balls).

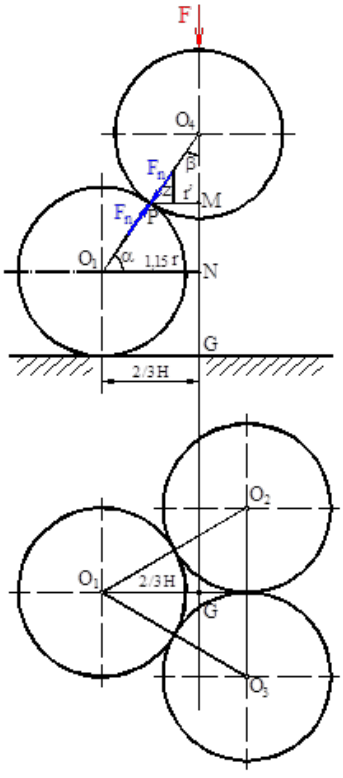

Fig. 5 The model geometry

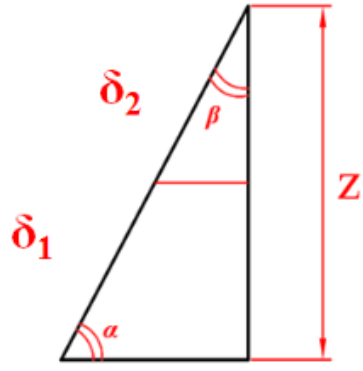

Fig. 6 Components of the vertical displacement z, as $z = (\delta_1+\delta_2)\times\sin\alpha$

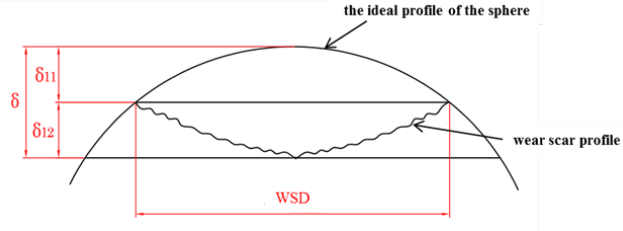

Fig. 7 Depth of wear scar, measured on the 2D profile, perpendicular to the sliding direction

The simulation has as variables the friction coefficient and the vertical displacement of the rotating ball, equivalent to the force applied in the actual test (Table 4). In Table 4, δ_{11} is the depth of the wear scar measured on the 2D profile of the fixed ball, δ_{12} is the height of the spherical cap (Fig. 7), which is calculated with the relation:

$$A=[\pi(WSD)^2]/4 \quad (2)$$

and the result is:

$$\delta=[\pi(WSD)^2]/8\pi r=(WSD)^2/8r \quad (3)$$

WSD is the average value of wear scar diameter obtained in [26] for a certain load and *r* is the ball radius.

Table 4. Measured and adopted values for z

Load (N)	WSD (μm)*	δ_{12} (μm) (profile depth under the midline)	δ_{11} (μm) (height of cap with WSD base)	δ_1 (μm)	$2\delta_1$ (μm)	z (μm)	z value (μm), applied in simulation
500	354	1.5	2.466	3.96685	7.933701	6.48	6.5
600	426	2.2	3.572	5.772362	11.54472	9.44	9.5
700	687	12	9.290	21.29073	42.58146	34.83	35
850	2582	220	131.234	351,2347	702.4694	574.62	575
900	2692	230	142.654	372,6548	745.3096	609.66	610

*These values were measured for four-ball tests, lubricated with rapeseed oil and with 1400 rot/ min, for 1 hour [26].

The centers of the three non-rotating balls on the actual tribotester, before loading, form an equilateral triangle $\Delta O_1O_2O_3$ (Fig. 5). The weight center of this triangle, denoted by G, is at the intersection of its heights, at 2/3 of the peak and at 1/3 of the base. The height of the equilateral triangle is

$$O_{1G}= 2/3\ H=1.15\times r \quad (4)$$

The approach of the two balls in the direction of their centers is considered to be a sum

$$\delta=\delta_{11}+\delta_{12} \quad (5)$$

where δ_{11} and δ_{12} are the changes of the simplified ball profiles on the radial direction. In turn, this consists of two components (Fig. 5):

- the depth of the wear scar measured on the 2D profile, perpendicular to the sliding direction,
- the height of the spherical cap, calculated as the average value for WSD, as measured for the same force in the actual test.

The simulated cases have as variable COF and the vertical displacement of the rotating sphere, which was introduced as a value of the vertical displacement taking into account the actual deformation of the balls.

The displacement of the rotating ball shall be calculated as the projection on the vertical direction of displacement δ and the angle α, between the vertical direction and the normal direction of the contact between two balls, the fixed one and the rotating one (Fig. 6).

Because δ_{11} and δ_{12} are difficult to be measured, they are calculated considering the average value of wear scar diameter on the stationary ball, as the diameter of a spherical cap, of height δ_{11} and δ_{12}, as measured from 2D profilometry on tested fixed balls, respectively:

$$z=2\delta\ sin54.90°=1.636\ \delta \quad (6)$$

$$\delta = z/(2\sin\alpha) \tag{7}$$

For the same value of δ, three cases are run, each with a different value for the friction coefficient. Table 5 shows the average diameters of the wear scars (WSD), the depth of the profile δ_{11}, obtained from the measurements and geometric parameters, so that the displacement z can be applied in the model. z represents the calculated values of the displacement, the last column of the table being the values applied in the simulations, approximated to the first decimal figure.

Fig. 8 gives the curve for the displacement z and it is observed that up to 800 N, the value of the displacement slightly increases but, from 850 N, the displacement has higher values, the very high jump being done between 800 N and 850 N.

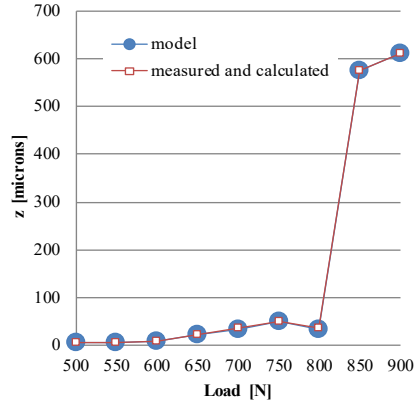

Fig. 8 The value of vertical displacement of the balls, corresponding to the force applied in vertical direction, in actual tests

Figure 9 presents 2D profiles of the wear scar on the non-rotating ball, perpendicular to the sliding direction, for different loads, from the smallest analyzed load, F = 500 N, to higher analyzed load, F = 850 N. It is observed that, for F = 500 N and for F = 700 N, the shape of the profile indicates a very small depth of the wear scar, the profile revealing rather superficial abrasive wear. For F = 750 N to F = 900 N, a much greater scar depth is observed (here only that for F = 850 N), without excessive abrasion on the surface, which would suggest a strong plastic strain and a lower intensity of abrasive wear.

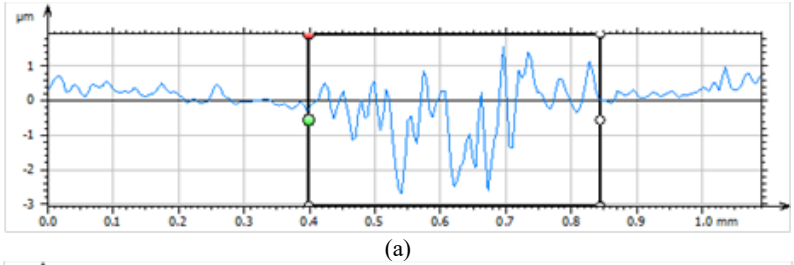

(a)

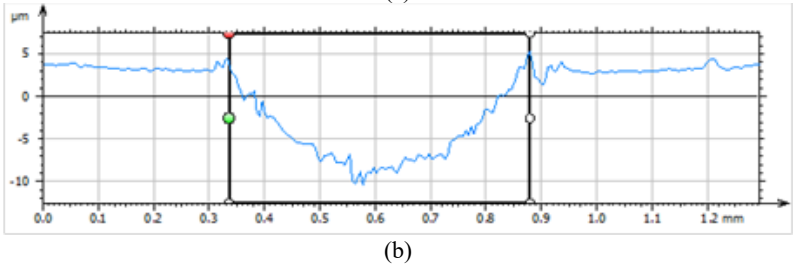

(b)

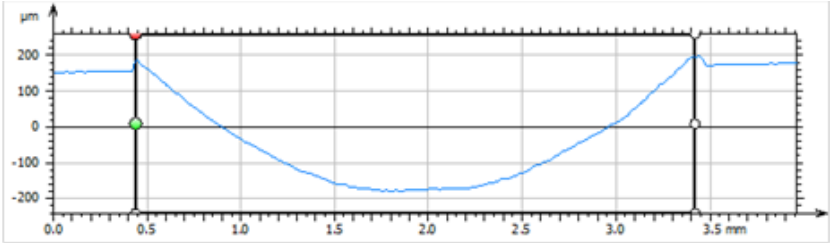

(c)

Fig. 9 Typical 2D profiles of the wear scar, measured perpendicular to the sliding direction, for the stationary ball: (a) F = 500 N, ball 1; (b) F = 700 N, ball 1; (c) F = 850 N, ball 1 (each figure has its own scale) (tests on four-ball tester, with rapeseed oil) [26]

3. SIMULATION RESULTS AND DISCUSSIONS

The Influence of the COF Value on Stress and Strain Distributions

The simulation of sliding was done for the following cases: without friction (COF = 0) and with friction (COF = 0.08 and COF = 0.1). For each case, the maximum equivalent stress in time is analyzed and the distributions of equivalent stress, total and plastic strains at the end of rotation are discussed. Fig. 10 shows the evolution of the maximum elastic strain in time, for two values of the applied loads (F = 500 N and F = 900 N), for the stage with sliding between the balls.

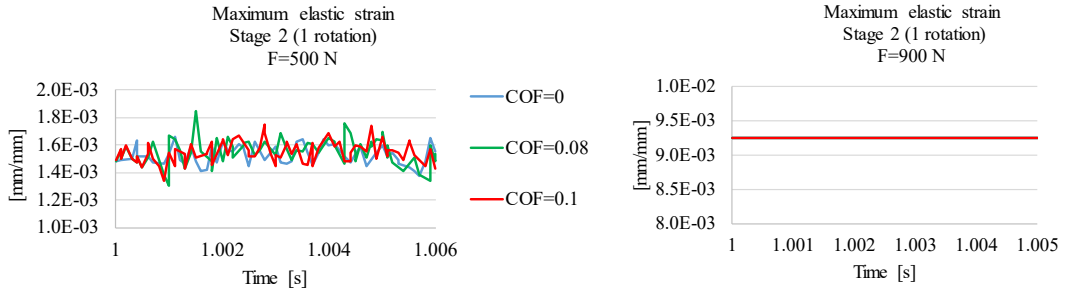

(a) (b)

Fig. 10 The evolution of the maximum elastic strain, on the stationary ball, in time, for the two values of the applied load. (a) F = 500 N (δ = 6.5 μm); (b) F = 900 N (δ = 610 μm)

Under lower load, values for elastic strain are varying in time, in a band of 1.4×10^{-3} to 1.8×10^{-3} (mm/mm), the friction coefficient having a poor influence, but for the simulation under the highest load, the maximum value of elastic strain is the same, regardless of the friction coefficient value, meaning that the contact works in the elasto-plastic domain. According to the theory presented in Frunza [1] and Crețu [30], the total strain can be considered the algebraic sum of elastic strain and plastic strain. Therefore, the components of the total strain for the second stage in simulating the sliding between the two balls, will be further analyzed. For F = 500 N, maximum value of elastic strain in time varies in a narrow range, characteristic for a sliding contact. For F = 900 N, for all values of COF, the maximum elastic strain remains constant, which means that the material has exhausted its linear elasticity domain and entered the plastic domain. The elastic component has a similar behavior regardless of the value of the friction coefficient. The rotating ball pushes the material, creating a material threshold in front of the indentation, over which it must pass. This process is specific only to the elastic domain of the material. On the first rotation, in time, several peaks of

maximum elastic strain were observed, especially for COF = 0. For F = 900 N, it is observed that the values of maximum elastic strain are constant, in every moment of sliding, suggesting that the maximum total strain will have a plastic component, this being logically based on the overlap on the elastic effect. During the rotation of the upper ball, the maximum plastic strain values are given in Fig. 11. At F = 500 N, the value of maximum plastic strain at the end of the rotation is ordered proportionally to the friction coefficient. So, the highest value of plastic strain on the non-rotating ball, after a rotation, was obtained for COF = 0.1.

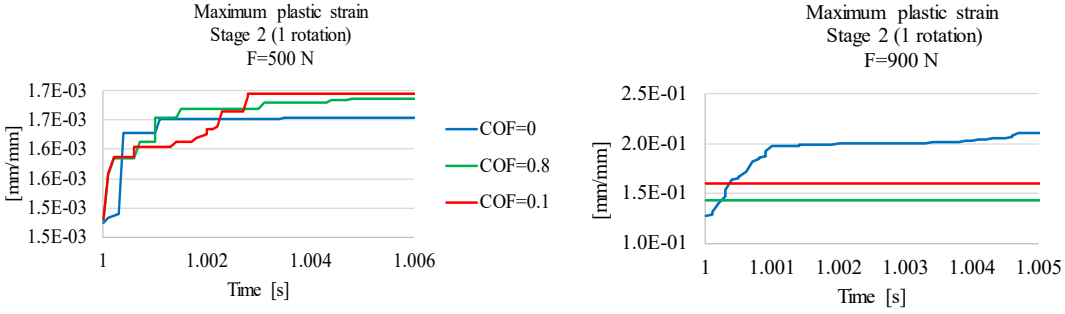

Fig. 11 Evolution of maximum plastic strain, on the fixed ball, in time, for stage 2 –rotation: (a) F = 500 N; (b) F = 900 N

Due to the lack of friction, the material in front of the contact may be more strongly deformed. The analysis of the simulation results is done by comparing the values of plastic strain to measured ones. It is observed that the model makes possible to notice very small values of plastic strain, difficult to measure (bellow 10^{-3} mm/mm). On any image with strain distribution, values between 3×10^{-3}… 4×10^{-3} mm/mm will be taken into account for measuring the strain contour on the model.

The higher friction coefficient causes an increase in plastic strain. The plastic strain may have close values, not necessarily in the order of increasing the friction coefficient from 0.08 to 0.1, but the differences are of the order of 10^{-5} mm/mm, which is a very small value.
The values of plastic strain already exceed 1/1000 of the ball diameter, so, F = 500 N is not in the load range for normal regime, already representing the start of a severe regime. The strain already appears, when the load is applied on the balls at rest, as it happens experimentally. The slight variations of the friction coefficient obtained experimentally can be explained by the small variations of elastic and plastic strains in time, as it happens in the simulation, too.
The maximum total strain in time is shown in Fig. 12 and it is based on the principle of overlapping effects, adding the elastic strain and the plastic strain.

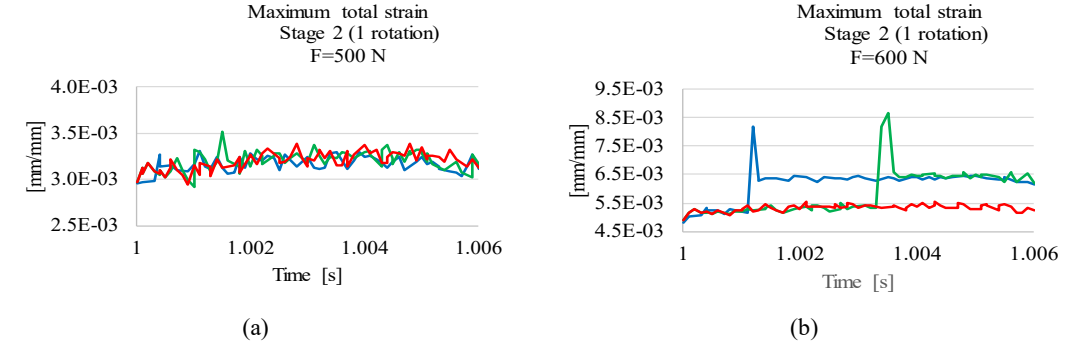

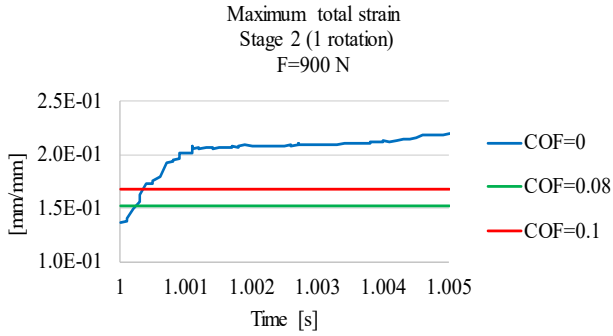

(c)

Fig. 12 Evolution of maximum total strain, in time, for the stage 2 (one rotation):
(a) F = 500 N; (b) F = 600 N; (c) F = 900 N

The analysis of the maximum values of the equivalent stress (von Mises) is given in Fig. 13. At F = 500 N, the range of variation of maximum von Mises stress in time is about the same, regardless of the value of friction coefficient. At F = 600 N, when the ball has done its statical imprint and must rotate, a maximum appears. Two stress peaks were observed, of about the same value (approximately 500 MPa) for COF = 0 and COF = 0.08. These could be explained by the fact that the upper ball has already imprinted the lower ball and, in rotation, it must pass over the edges of the imprint. For F = 500 N and F = 600 N, the maximum values of equivalent stress do not exceed the yield strength. The peaks of maximum equivalent stress correspond to the peaks of maximum total strain.

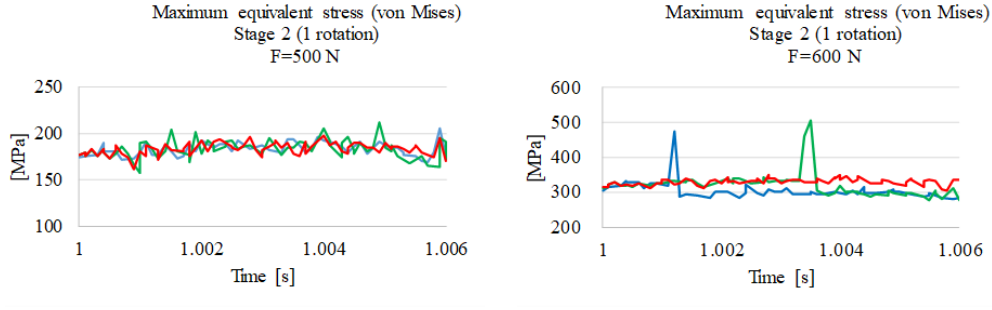

(a) (b)

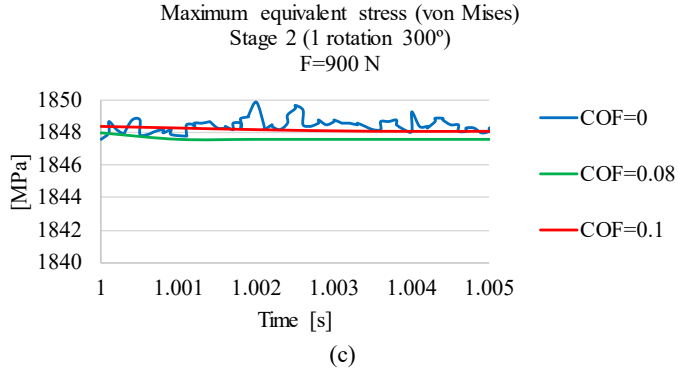

(c)

Fig. 13 The evolution of the maximum equivalent stress in time, for the stage 2 (one rotation):
(a) F = 500 N; (b) F = 600 N; (c) F = 900 N

For F = 900 N, the equivalent stress is constant because the imprint increases by plastic deformation. For higher values of the friction coefficient, a smaller variation of the equivalent stress is noticed. The variation of the maximum values of the equivalent stress for the case without friction, during rotation, is 0.119% of the minimum value recorded for this case and calculated with

$$\frac{\sigma_{max} - \sigma_{min}}{\sigma_{min}} \cdot 100\ [\%] \tag{8}$$

Table 5 presents the calculated values of the displacement, the average diameters of the wear scars, measured with the help of an optical microscope [26], but also on the model for all applied forces. Table 6 gives the maximum and minimum values of equivalent stress (von Mises) and their variation in time (during the rotation), for the simulated cases, having as variables the force and the friction coefficient.

The percentage variation of maximum equivalent stress during rotation is the ratio between the variation of equivalent stress and the maximum equivalent stress during the analyzed time interval and it is calculated by the formula:

$$\Delta\sigma_{\%} = \frac{\Delta\sigma}{\sigma_{max}} \cdot 100\ [\%] \tag{9}$$

where $\Delta\sigma$ is the difference between the maximum value of the equivalent stress (σ_{max}) in time and the minimum value obtained for the equivalent stress (denoted σ_{min}), for the same time interval (a rotation).

Table 5. Measured wear scar diameters (WSDs), displacement and ~~average~~ variation of WSDs.

Case	Load on actual system (N)	z (mm)	Measured WSD (average for one test) (mm)	Measured WSD on the model (mm)	Average variation (%) $\frac{WSD_{real} - WSD_{model}}{WSD_{real}} \cdot 100$
1	500	0.0065	0.354 (0.298…0.389)	0.4 (0.390…0.410)	-13
2	600	0.0095	0.426 (0.397…0.423)	0.440 (0.420…0.455)	-3
3	700	0.035	0.687 (0.63…0.744)	0.700 (0.680…0.720)	-2
4	850	0.575	2.582 (2.5…2.65)	2.750 (2.6…2.8)	-7
5	900	0.61	2.692 (2.569…2.883)	2.800 (2.7…2.9)	-4

Table 6. The variation of equivalent stress, depending on the load and COF

Load (N)	COF	σ_{max} (MPa)	σ_{min} (MPa)	$\Delta\sigma$ (MPa)	$\Delta\sigma_{\%}$ [%]
500	0	205	170	35	17.07
	0.08	210	158	52	24.76
	0.1	197	161	36	18.27
900	0	1850	1833	17	0.91
	0.08	1848	1833	15	0.81
	0.1	1848	1830	18	0.97

The Influence of Load on the Model Behavior

Figure 14 presents the evolution in time of maximum values of von Mises stress, during the simulated rotation. In the already-loaded ball rotation (stage 2 of the simulation), in the time

interval (0-1.005 s), for both cases, without and with friction (COF = 0 and COF = 0.1), at lower loads (F = 500 N and F = 600 N), in time, maximum values of von Mises stress vary in a small range, being lower for the lower load. The graphs for these cases are similar, stress values not exceeding the value of the yield limit.

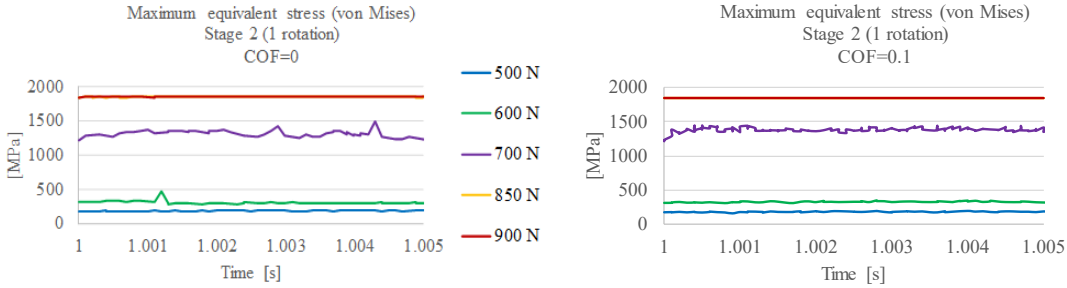

Fig. 14 The influence of the friction coefficient on the evolution of maximum equivalent stress in time, during stage 2 (one rotation): (a) COF = 0; (b) COF = 0.1

For F = 700 N, for both cases, with and without friction, the varying stress interval is about the same, the maximum value of the equivalent stress reaching 1500 MPa. For F = 850 N and F = 900 N, the maximum value of the equivalent stress is close to 1850 MPa, the strength limit of the ball material, meaning the plastic strain takes place.

The influence of the load on the maximum elastic strain evolution in time, during rotation, is given in Fig. 15. Peaks of elastic strain, for F = 600 N and F = 700 N are observed, resulting from local deformation of the material, at that moment. In the cases with friction, a scratch of the graph of maximum values of elastic strain in time, for F = 600 N and F = 700 N, is noticed. For F = 850 N and F = 900 N, the graphs are perfectly superimposed on each other, meaning that maximum value of the elastic strain was reached.

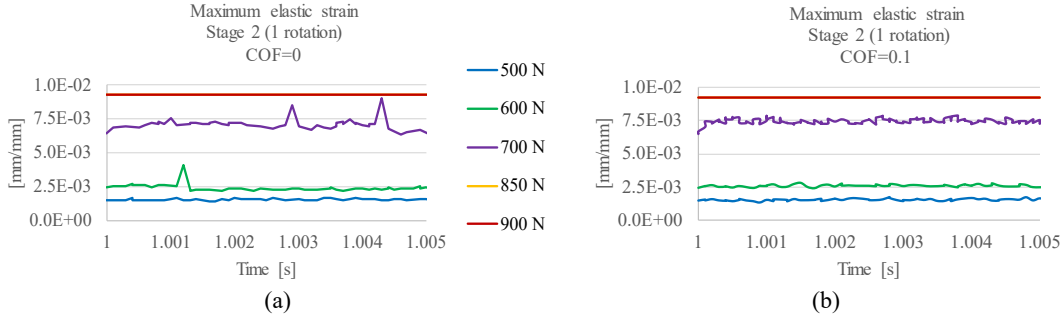

Fig. 15 Influence of COF on the distribution of maximum elastic strains in time, for stage 2, during rotation: (a) COF = 0; (b) COF = 0.1

Figure 16 shows the influence of load on maximum plastic strain. For forces of 500 N, 600 N and 700 N, it is noticed a similar evolution, for both cases (with and without friction). However, for F = 700 N, slightly higher values of maximum plastic strain are observed than those for the loads F = 500 N and F = 600 N. At high loads, much higher values of plastic strain are observed, reaching 2.5×10^{-1} mm/mm for the case without friction. The maximum plastic strain is higher in the case without friction than that in the case with friction (COF ≠ 0).

Figure 17 shows how the friction coefficient influences the distribution of equivalent stresses at the end of the rotation, only for the cases COF = 0 and COF = 0.1, for the load F = 500 N. The equivalent stress values for both simulated cases are relatively close.

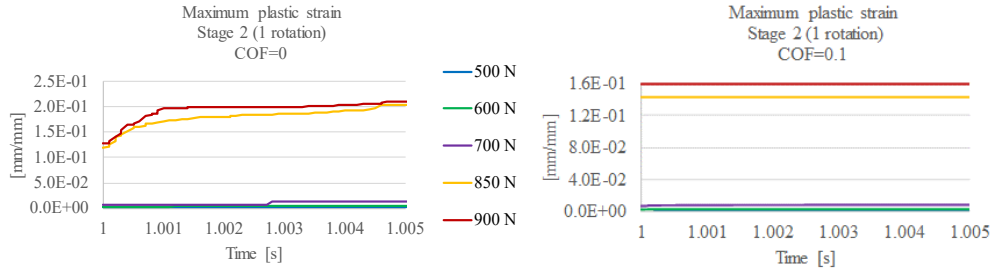

(a) (b)

Fig. 16 Influence of COF on maximum plastic strain, stage 2 (during rotation): (a) COF = 0; (b) COF = 0.1

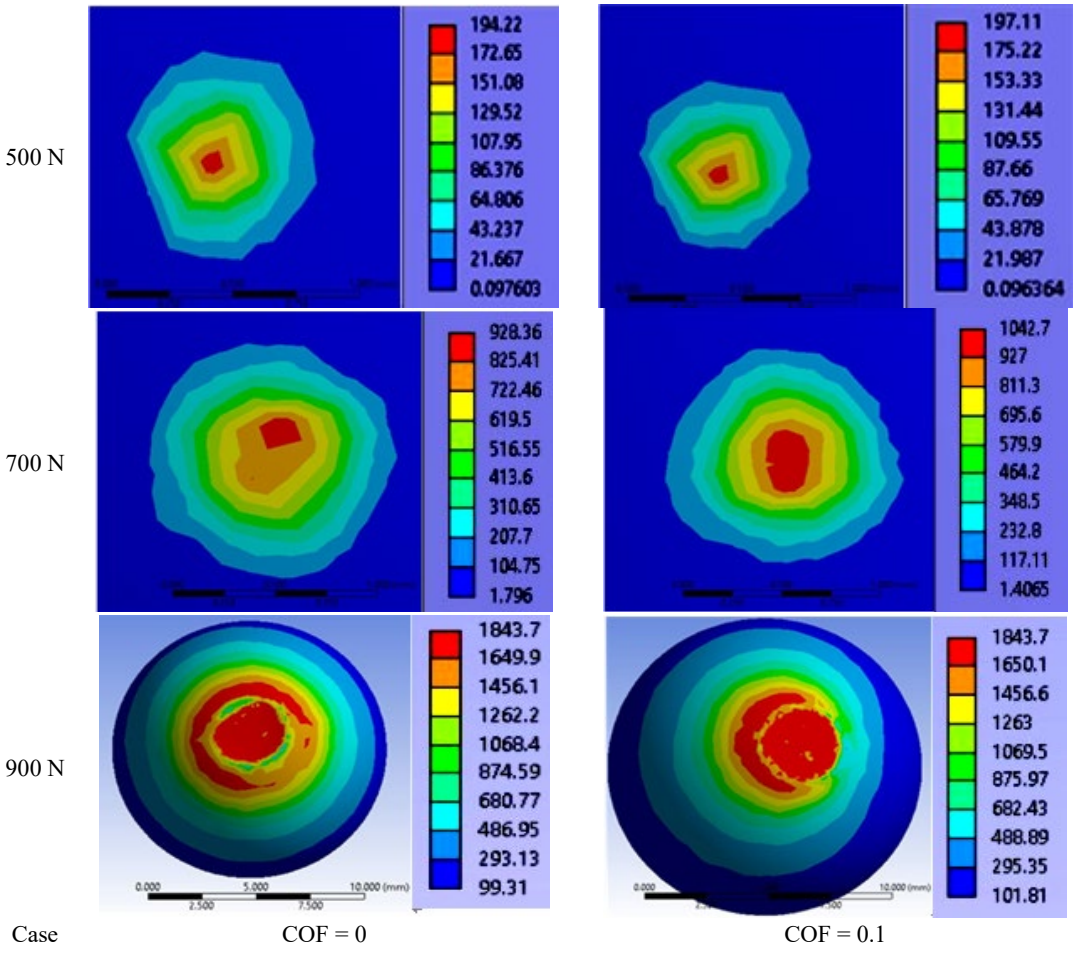

Fig. 17 Influence of friction coefficient on the distribution of equivalent stress (in MPa), on the stationary ball, for F = 500 N, F = 700 N and F=900 N. The rotating ball performed an angle of rotation equal to 360º for F = 500 N and F = 700 N and 300º for F = 900 N

For F = 700 N, the values of maximum equivalent stress reach ~1042.7 MPa for the stationary ball, obviously a value near the yield limit. In both cases, with and without friction, for F = 900 N, the value of the equivalent maximum stress is 1843.7 MPa, being above the yield value introduced for the constitutive model of ball steel and very close to the strength limit of ball material. Figure 18 presents wear scars, virtually re-built with the Mountains SPIP 8.1 software,

for one ball, non-rotating, of a set of balls tested in non-additivated rapeseed oil. The test was done for loads of 500 N, 850 N and 900 N, and the sliding speed was 0.53 m/s. The testing time was 60 s, and the test regime was severe. The wear scars on the fixed balls are not symmetrical, the explanation being the position of the balls in the tribotester and the sliding direction. For high loads, the 3D profilometry shows large plastic strains.

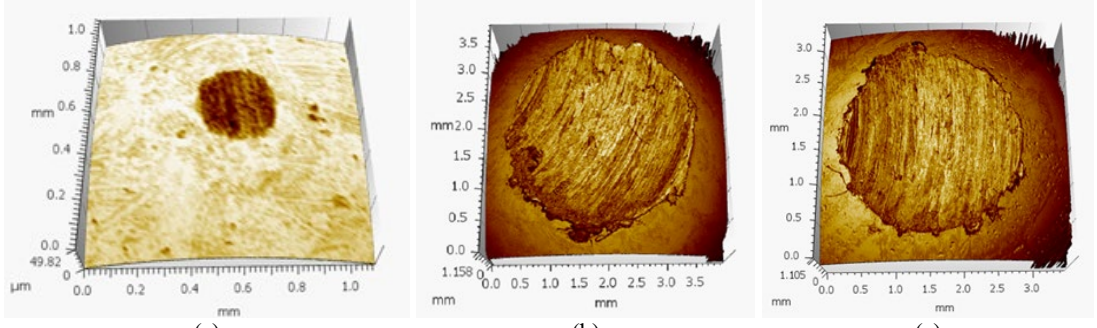

Fig. 18 Wear scars, virtually re-built with the Mountains SPIP 8.1 software, on the stationary ball: (a) F = 500 N; (b) F = 850 N; (c) F = 900 N [26]

Figure 19 presents the total strain distributions on the contact zone of fixed ball, and how they were influenced by the friction coefficient (for COF = 0 and COF = 0.1). The simulation was performed for a load F = 500 N, for these two cases. In the first case, there was no friction and in the second, a friction coefficient equal to 0.1 was taken into account. The distributions of total strain, for the second stage are given for the second stage of simulation, at the end of simulation, when the upper ball rotates for an angle of 360°. It can be seen that the values of the total strain are quite small. Higher values of the total strains are observed on the stationary ball in the case with COF = 0 and F = 900 N.

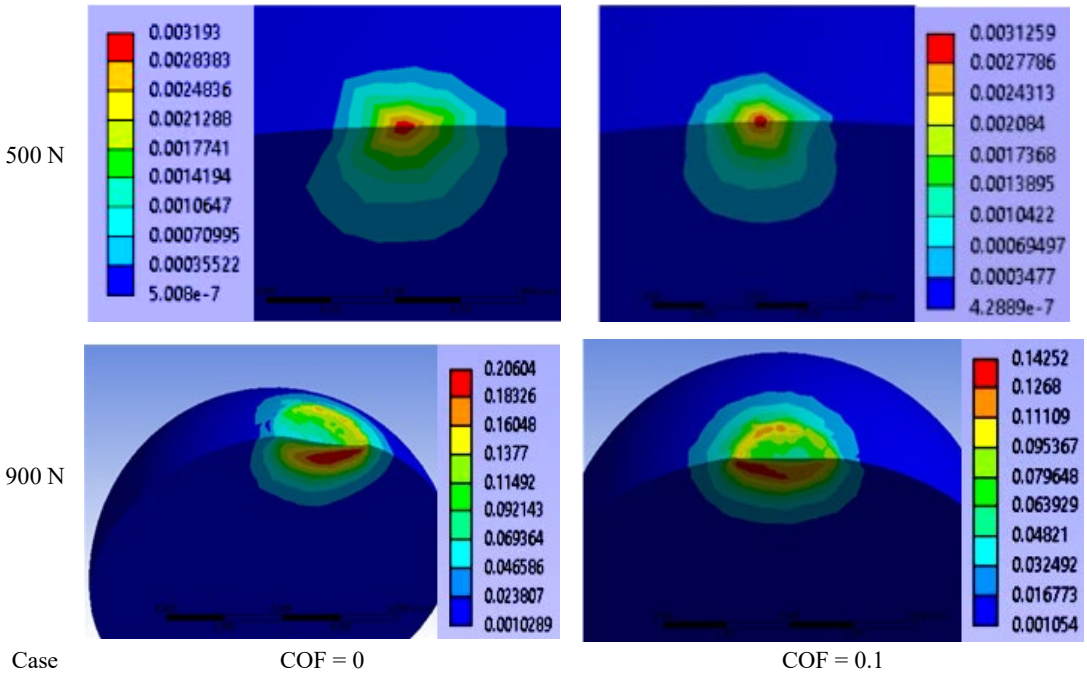

Fig. 19 Influence of the friction coefficient (COF) on the distribution of the total strain (mm/mm), on the stationary ball, for F = 500 N. The rotating ball performed an angle of rotation equal to 360º.

Figure 20 presents images with isolines of plastic strains for fixed ball, for the simulated loads F = 500 N and F = 900 N, in case without friction, but also in case with friction. Isolines of 0.0007 mm/mm (for F = 500 N) and 0.06 mm/mm (for F = 900 N) approximatively have dimensions corresponding for the average value of wear scar diameters, as measured after actual tests in [24, 27, 28].

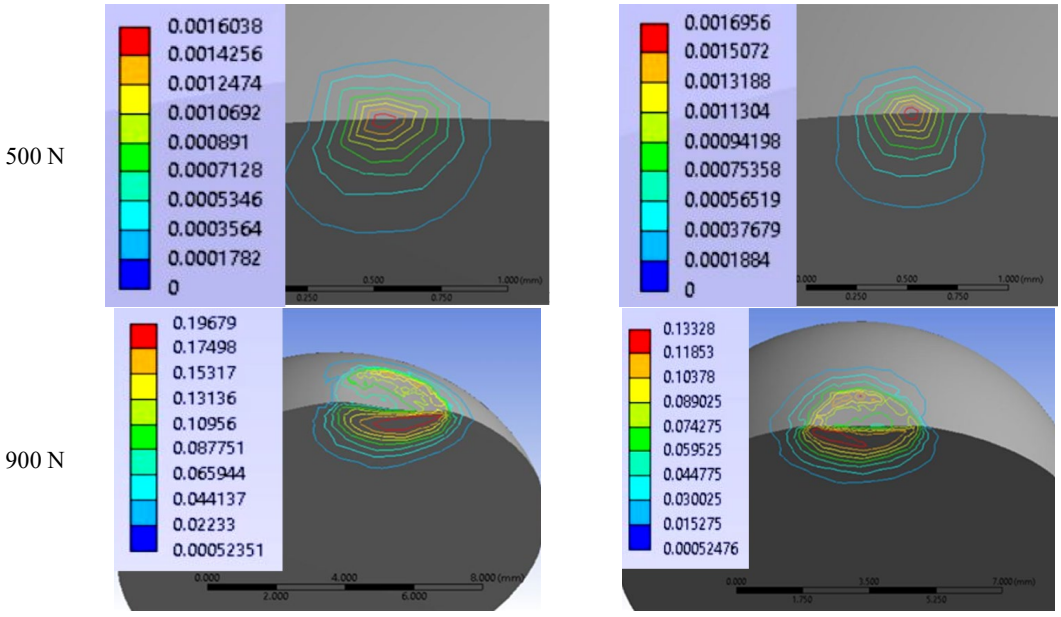

Fig. 20 Distribution of plastic strains (isolines), for F = 500 N and for F = 900 N, in mm/mm

4. CONCLUSIONS

The model is an original simplified finite element model of the four-ball tribotester. The simulation is done in two steps. The first step consists of the static loading on the two balls, based on a calculated and measured approach corresponding to each load in the severe regime), and in the second step, a partial rotation (300°), or complete rotation (360°) is done. The material constitutive model takes into account experimental data obtained on the same steel grade, 100Cr6, with the same quality in terms of hardness, Young's modulus and equivalent plastic strain at break.

The model is useful for evaluating the stress and strain distributions, so that a working range for test parameters and the transition from normal regime (acceptable load in operation) to a severe regime (by identifying maximum equivalent stress close to yield point or strength limit) can be evaluated. Qualitatively, the model highlights the ellipsoidal shape of the ball indentation due to the influence of frictional loading and the sliding movement.

In this model, wear was not simulated and surfaces in contact are perfectly smooth, but in reality, abrasive wear dominates in the normal regime, in the severe regime being dominant plastic strain processes (similar to those in simulation) and adhesive wear that is not highlighted by simulation.

ACKNOWLEDGMENTS

An earlier version of this work was orally presented at the 10th International Conference on Tribology –BALKANTRIB '20 (20–22 May 2021, Belgrade, Serbia) by the same authors. The present paper represents a substantially extended and refined version of that contribution.

REFERENCES

[1] G. Frunza and S. Spinu, *Fundamentele teoriei plasticității. Aplicații în mecanica contactului elasto-plastic*, Suceava (Romania): Editura Universității "Stefan cel Mare", 2010.
[2] K. L. Johnson, *Contact Mechanics*, Cambridge (UK): Cambridge University Press, 1985.
[3] S. D. Mesarovic and K. L. Johnson, Adhesive contact of elastic–plastic spheres, *J Mech Phys Solids*, **48**(10): 2009-2033 (2000).
[4] M. R. W. Brake, An analytical elastic plastic contact model with strain hardening and frictional effects for normal and oblique impacts, *Int J Solids Struct,* **62**: 104-123 (2015).
[5] N. H. Nazir, A. K. Zulfiqar, S. Adil, Experimental analysis and modelling of c-crack propagation in silicon nitride ball bearing element under rolling contact fatigue, *Tribol Int*, **126**: 386-401 (2018).
[6] Ł. Szparaga, P. Bartosik, A. Gilewicz, K. Mydłowska, J. Ratajski Optimisation of mechanical properties of gradient Zr–C coatings, *Materials*, **14**, 296, https://doi.org/10.3390/ma14020296, 2021.
[7] M. Sofonea, A. Matei, *Mathematical Models in Contact Mechanics*, **111-113**, 173-216, Cambridge (UK): Cambridge University Press, 2012.
[8] V. A. Yastrebov, *Numerical Methods in Contact Mechanics*, Hoboken (New Jersey, USA) ISTE Ltd John Wiley & Sons, Inc., 2013.
[9] B. Chatterjee, P. Sahoo, Elastic-plastic contact of a deformable sphere against a rigid flat for varying material properties under full stick contact condition, *Tribology in Industry*, **33**(4): 164-172, 2011.
[10] J. R. Barber, *Contact Mechanics*, Cham (Switzerland): Springer International Publishing AG, 2018.
[11] S. L. Yan, L.Y. Li, Finite element analysis of cyclic indentation of an elastic-perfectly plastic half-space by a rigid sphere, *Proc Inst Mech Eng C J Mech Eng Sci*, **217**(5): 505-514, 2003.
[12] L. Li, I. Etsion, F. E. Talke, Elastic–plastic spherical contact modeling including roughness effects, *Tribol Lett*, **40**: 357–363, 2010.
[13] H. Ghaednia, X. Wang, S. Saha, Y. Xu, A. Sharma, R. L. Jackson, A Review of elastic–plastic contact mechanics, *Appl Mech Rev*, **69**(6), 060804, 2017.
[14] O. Bartier, X. Hernot, G. Mauvoisin, Theoretical and experimental analysis of contact radius for spherical indentation, *Mech of Mater*, **42**(6): 640–656, 2010.
[15] V. S. N. Karthik, Finite element analysis of spherical indentation to study pile-up/sink-in phenomena in steels and experimental validation, *Int J Mech Sci*, **54(**1): 74-83, 2012.
[16] Y. Wen, J. Y. Tang, A solution considering elastic-plastic deformation of asperities for contact between rough cylindrical surfaces, *Industrial Lubrication and Tribology*, **70**(2), https://doi.org/10.1108/ILT-09-2017-0269, (2018).
[17] P. G. Nikolakopoulos, K. Grigoriadis, A. Zavos, Contact modeling with a finite element model in piston ring–liner conjunction under dry conditions, *Int J Struct Integr*, **10**(3), https://doi.org/10.1108/IJSI-10-2018-0076, 2019.
[18] R. Yu, W. Chen, Fractal modeling of elastic-plastic contact between three-dimensional rough surfaces, *Industrial Lubrication and Tribology*, **70**(2): 290-300, https://doi.org/10.1108/ILT-02-2017-0048, 2018.
[19] C. Hornton, *Granular Dynamics, Contact Mechanics and Particle System Simulations*, https://doi.org/10.1007/978-3-319-18711-2, Cham (Switzerland): Springer International Publishing AG, 2015.
[20] K. L. Johnson, J. A. Greenwood, J. G. Higginson, The contact of elastic regular wavy surfaces, *Int J Mech Sci*, **27**(6): 383-396 (1985).
[21] J. Zhao, Q. Kan, P. Fu, G. Kang, P. Wang, An elasto-plastic contact solving method for two spheres, *Acta Mech Solida Sin*, **33**(5): 612–634, 2020.
[22] C. Hardy, C. N. Baronet, G. V. Tordion, The elasto-plastic indentation of a half-space by a rigid sphere, *Int J Numer Methods Eng INT J NUMER METH ENG*, **3**(4): 451-462 (1971).
[23] M. M. David, *The tribological effects of lubricating oil containing nanometer-scale diamond particles*, Ph.D. Thesis, New York City (USA): Columbia University, 20https://doi.org/10.7916/D8FF3R6G, 2015.
[24] G. C. Cristea, *Tribological characterization of soybean oil additivated with nanomaterials based on carbon (black carbon, graphite, graphene)*, Ph.D. Thesis. Galati (Romania): Dunarea de Jos University, 2017.

[25] C. Georgescu, L. Deleanu, C. G. Cristea, The tribological behavior of soybean oil, In *Soybean - Biomass, Yield and Productivity,* Kasai M. Ed., London (UK): IntechOpen Limited, DOI: 10.5772/intechopen.81234, 2018.
[26] T. F. Ionescu, *A tribological study of lubricants based on rapeseed oil and nano additives for reducing friction and wear*, Ph.D. Thesis, Galati (Romania): Dunarea de Jos University, 2021.
[27] J. Salençon, *Elastoplastic Modeling*, 16-76, Hoboken (New Jersey, USA): ISTE Ltd, John Wiley & Sons Inc., 2020.
[28] Y. B. Guo, C. R. Liu, Mechanical properties of hardened AISI 52100 steel in hard machining processes, *J Manuf Sci Eng*, **124**(1): 1-9 (2002).
[29] L. C. Şolea, *Contributions on studying the rheological and tribological behavior of several biodegradable lubricants based on vegetal oils*, Ph.D. Thesis, Galati (Romania): Dunarea de Jos University, 2013.
[30] S. Cretu, *Contactul concentrat elastic-plastic*, Iasi (Romania): Editura Politehnium (2009).